Noname manuscript No.
(will be inserted by the editor)

A Variational Approach to Estimate Incompressible Fluid Flows.

Praveen Chandrashekar, Souvik Roy,
A. S. Vasudeva Murthy

the date of receipt and acceptance should be inserted later

Abstract A variational approach is used to recover fluid motion governed by Stokes and Navier-Stokes equations. Unlike previous approaches where optical flow method is used to track rigid body motion, this new framework aims at investigating incompressible flows using optical flow techniques. We formulate a minimization problem and determine conditions under which unique solution exists. Numerical results using finite element method not only support theoretical results but also show that Stokes flow forced by a potential are recovered almost exactly.

Keywords variational, incompressible, finite element, optical flow, Stokes, Navier-Stokes.

Mathematics Subject Classifications 76M

1 Introduction

Our motivation for the present study is to understand cloud motion from satellite images. This in turn will help us in understanding the movement of rain bearing clouds during the monsoon over the Indian subcontinent. Previous work in this direction are [1–5]. The methodology is to obtain fluid flow estimates from given image sequences by incorporating physical constraints into a variational approach to optical flow method (OFM). However, a major problem in applying OFM to fluid flow, leave alone cloud motion is that the connection between optical flow in the image plane and fluid flow in the 3D

Praveen Chandrashekar, Souvik Roy, A. S. Vasudeva Murthy
TIFR Center for Applicable Mathematics,
Bangalore-560065,
India.
Tel.: (080)6695-3719, +91 9035287250,(080)6695-3738.
Fax: (080)6695-3799.
E-mail: (praveen,souvik, vasu)@math.tifrbng.res.in

world is yet to be understood satisfactorily [6]. Given this state of affairs we propose to apply OFM to images that are generated synthetically by solving the 2D incompressible Stokes and Navier Stokes equation. Our aim is to track movement of vortex structures generated by solving the 2D incompressible Stokes and Navier-Stokes equation. In the context of optical flow methods the first major known work is the Horn-Schunck algorithm, which implements a constraint free first order regularization approach with a finite differencing scheme [7]. The method was devised to capture rigid body motion. There are no fluid flow constraints. The first known related work of applying OFM to estimate fluid flow is [8]. The authors estimate optical flow involving prior knowledge that the flow satisfies Stokes equation. They formulate a minimization problem based on the Horn-Schunck functional and determine the optimal source term and the boundary velocity coming from a incompressible Stokes equation to recover the flow completely. While this approach is suitable if not much is known about the flow, it restricts the class of recovered incompressible flows to only Stokes flow. The second work connecting OFM to fluid flow is [9]. The authors minimize the Horn-Schunck functional with higher order regularization incorporating the incompressibility constraint coupled with mimetic finite differencing scheme. Such an approach with higher regularization term turns out to be costly and it increases the regularity of the fluid velocity field, which is not the case in usual flows. Motivated by these works, our aim is to investigate a class of incompressible flows using OFM. We do not constrain our flow to be Stokes flow as in [8] or use higher order regularization terms as in [9]. Instead a minimization problem is formulated based on the Horn-Schunck functional and the incompressibility constraint. An extensive analysis has been performed on our OFM to show that one can recover a class of Stokes flow exactly. This approach can then be extended to recover even Navier-Stokes flows.

It is well known [7] that tracking rigid body motion by OFM can be done satisfactorily using nonlinear least squares technique whereas it is totally inadequate for fluid flow [10]. This is because rigid body motion has features like geometric invariance where local features such as corners, contours etc., are usually stable over time [11]. However, for fluid images these features are difficult to define leave alone being stable. This is one of the main problems in understanding the connection between optical flow and fluid flow [12–15]. To recover fluid-type motions, a number of approaches has been proposed to integrate the basic optical flow solution with fluid dynamics constraints, e.g., the continuity equation that describes the fluid property [14, 16] or the divergence-curl (div-curl) equation [14, 17] to describe spreading and rotation. The main aim of our work is to track fluid flow at each instant of time by tracing passive scalars which are propagated by the flow using simple flow dynamics and specifying appropriate boundary conditions. In other words, we use optical flow techniques to efficiently track fluid flow motion. Such a work has its importance in determining atmospheric motion vectors (AMV), tracking smoke propagation, determining motion of tidal waves using floating buoys. Since the basic idea in the variational approach is not to estimate locally and individually but to estimate non-locally by minimizing a suitable functional defined over the entire image section, we therefore prefer a variational approach.

The paper is organised as follows. In Section 2, a minimization problem is formulated with a first order regularization term under the incompressibility constraint. In Section 3, we derive conditions on the image under which unique solution exists. Section 4 presents an outcome of the present work which shows when the real unknown flow observed through images comes from a Stokes flow forced by a potential, then we are able to recover the velocity almost exactly even for very small viscosity coefficient. In Section 5, continuous Galerkin finite element method is used to solve the resulting set of equations using FENICS [18]. The reason for using finite element method for the variational model arises from the fact that the numerical experiments done with finite element method for the Horn-Schunck model to track underlying flows gave excellent results [19]. Section 6 investigates motion satisfying Stokes and Navier-Stokes flows by performing numerical experiments on four test cases for low and high Reynolds number flows. Section 7 summarizes the results obtained.

2 Variational Formulation

To estimate fluid flow, we trace passive scalars that are propagated by the flow. Examples of such scalars are smoke, brightness patterns of dense rain-bearing clouds whose intensity remains constant atleast for a short time span. These scalars can be represented by a function $E : \Omega \times \mathbb{R}^+ \longrightarrow \mathbb{R}$ so that $E(x,y,t)$ for $(x,y) \in \Omega$ represents a snapshot of the image of the scalars at time $t \in \mathbb{R}^+$. Here Ω is a bounded convex subset of $\mathbb{R}^2$. Let us assume our image $E(x,y,t) \in W^{1,\infty}(\Omega)$, for each t and hence in $L^2(\Omega)$ (as Ω is bounded). Let the field of optical velocities over Ω at a fixed time $t = t_0$ be $U(x,y,t_0) = (u,v)(x,y,t_0)$ and $X = (H^1(\Omega))^2$. Define the functional,

$$J(U) = \frac{1}{2}\int_\Omega (E_t + U \cdot \nabla E)^2 dxdy + \frac{K}{2}\int_\Omega \|\nabla U\|^2 dxdy, \quad K > 0 \qquad (1)$$

where E_t and ∇E are evaluated at $t = t_0$, and

$$\|\nabla U\|^2 = \|\nabla u\|^2 + \|\nabla v\|^2.$$

Without loss of generality, let $t_0 = 0$. The first term in (1) represents the constant brightness assumption of the tracers. The second term represents a regularization term for the flow velocities. Such a functional was first considered by Horn and Schunck[7] and subsequently by many others [24–27, 12, 28] to efficiently estimate rigid body motion. Here it is used to track the underlying fluid flow motion. Such a connection between optical flow and fluid flow tracking is essential because if a proper connection is found, techniques from optical flow to determine high-resolution velocity fields from various images in continuous patterns can then be used. To use (1) to track fluid flows, we need to include fluid dynamics and enforce proper boundary conditions. Hence, we enforce the incompressible fluid flow constraint

$$\nabla \cdot U = 0. \tag{2}$$

The minimization problem can be stated as

$$\min_{U \in X} \quad \{J(U) |\ \nabla \cdot U = 0\}. \tag{P}$$

The boundary conditions on the flow velocity could be either Dirichlet or Neumann.

3 Existence and Uniqueness Of Minimizer

We show existence and uniqueness of minimizer for the Problem (P). Before that we state some standard definitions and results.

3.1 Preliminary Results

Let $(Z, \|\cdot\|_Z)$ be a Banach space.

Theorem 1 *Let $J : Z \to \mathbb{R} \cup \{-\infty, \infty\}$ be a convex functional on Z. If J is bounded from above in a neighbourhood of a point $U_0 \in Z$, then, it is locally bounded i.e., each $U \in Z$ has a neighbourhood on which J is bounded.*

Definition 1 A functional J defined on Z is said to be **locally Lipschitz** if at each $U \in Z$ there exists a neighbourhood $N_\epsilon(U)$ and a constant $R(U)$ such that if $V, W \in N_\epsilon(U)$, then

$$|J(V) - J(W)| \leq R\|V - W\|_Z.$$

If this inequaltiy holds throughout a set $Y \subseteq Z$ with R independent of U, then we say that J is **Lipschitz** on Y.

Theorem 2 *Let J be convex on Z. If J is bounded from above in a neighbourhood of one point of X, then J is locally Lipschitz in Z.*

Theorem 3 *Let J be convex on Z. If J is bounded from above in an neighbourhood of one point of Z, then J is continuous on Z.*

Theorem 1, 2, 3 and Definition 1 can be found in [29]. The following theorem from [20] is used to establish an unique global minimizer for (P).

Theorem 4 (Existence and uniqueness of global minimizer) *Let $J : Z \to \mathbb{R} \cup \{-\infty, \infty\}$ be a lower semi-continuous strictly convex functional. Also, let J be coercive i.e.,*

$$\lim_{\|U\|_Z \to +\infty} J(U) = \infty.$$

Let C be a closed and convex subset of Z. Then J has a unique global minimum over C.

Let us now verify the conditions stated in Theorem (4) for the functional J in (1). Let $H = L^2(\Omega)$, $H_1 = (L^2(\Omega))^2$ and $Z = X$ with norms $\|U\|_H = \|u\|_{L^2(\Omega)} + \|v\|_{L^2(\Omega)}$ and $\|U\|_Z = \|u\|_{H^1(\Omega)} + \|v\|_{H^1(\Omega)}$.

Theorem 5 *The functional given in (1) is strictly convex with respect to U under the assumption that E_x and E_y are linearly independent.*

Proof Let $U_1 = \begin{pmatrix} u_1 \\ v_1 \end{pmatrix}$ and $U_2 = \begin{pmatrix} u_2 \\ v_2 \end{pmatrix}$ where $(\cdot)$ is the usual inner product on $\mathbb{R}^2$. Then, for $0 < \alpha < 1$ and $U_1 \neq U_2$, we have

$$\begin{aligned} J(\alpha U_1 + (1-\alpha)U_2) &= \frac{1}{2}\int_\Omega ((\alpha U_1 + (1-\alpha)U_2)\cdot \nabla E) + E_t)^2 dxdy \\ &\quad + \frac{K}{2}\int_\Omega \left[\|\nabla(\alpha u_1 + (1-\alpha)u_2)\|^2 + \|\nabla(\alpha v_1 + (1-\alpha)v_2)\|^2\right] dxdy \\ \leq \frac{1}{2}\int_\Omega &\left[\{(\alpha U_1 + (1-\alpha)U_2)\cdot\nabla E\}^2 + 2E_t^2 + 2E_t\{(\alpha U_1 + (1-\alpha)U_2)\cdot\nabla E\}\right] dxdy \\ &\quad + \frac{K}{2}\int_\Omega \left[\|(\alpha\nabla u_1 + (1-\alpha)\nabla u_2)\|^2 + \|(\alpha\nabla v_1 + (1-\alpha)\nabla v_2)\|^2\right] dxdy. \end{aligned}$$

Let $a, b \in \mathbb{R}$ and A, $B \in \mathbb{R}^2$, with inner product

$$(A, B) = A_1B_1 + A_2B_2$$

and norm

$$\|A\|^2 = A_1^2 + A_2^2$$

where $A = (A_1, A_2)$ and $B = (B_1, B_2)$.
Then, for $0 \leq \alpha \leq 1$, we have,

$$\begin{aligned} [\alpha a + (1-\alpha)b]^2 &= \alpha^2a^2 + (1-\alpha)^2b^2 + \alpha(1-\alpha)2ab \\ &\leq \alpha^2a^2 + (1-\alpha)^2b^2 + \alpha(1-\alpha)(a^2+b^2), \\ &\qquad\qquad \text{(by Young's inequality)} \\ &= \alpha a^2 + (1-\alpha)b^2, \end{aligned}$$

where equality holds iff $a = b$ and,

$$\begin{aligned} \|(\alpha A + (1-\alpha)B)\|^2 &= \alpha^2\|A\|^2 + (1-\alpha)^2\|B\|^2 + \alpha(1-\alpha)\cdot 2(A,B) \\ &\leq \alpha^2\|A\|^2 + (1-\alpha)^2\|B\|^2 + \alpha(1-\alpha)(\|A\|^2 + \|B\|^2) \\ &\qquad\qquad \text{(by Young's inequality)} \\ &= \alpha\|A\|^2 + (1-\alpha)\|B\|^2, \end{aligned}$$

where equality holds iff $A = B$.
Thus,

$$\begin{aligned} &\frac{K}{2}\int_\Omega \left[\|(\alpha\nabla u_1 + (1-\alpha)\nabla u_2)\|^2 + \|(\alpha\nabla v_1 + (1-\alpha)\nabla v_2)\|^2\right] dxdy \\ \leq &\frac{K}{2}\left(\alpha\int_\Omega \left[\|\nabla u_1\|^2 + \|\nabla v_1\|^2\right] dxdy + (1-\alpha)\int_\Omega \left[\|\nabla u_2\|^2 + \|\nabla v_2\|^2\right] dxdy\right), \end{aligned} \tag{3}$$

and

$$\int_{\Omega} [(\alpha U_1 + (1-\alpha)U_2) \cdot \nabla E]^2 \, dxdy \leq \alpha \int_{\Omega} (U_1 \cdot \nabla E)^2 dxdy \\ +(1-\alpha) \int_{\Omega} (U_2 \cdot \nabla E)^2 dxdy. \tag{4}$$

Equality holds in (3) iff

$$\nabla u_1 = \nabla u_2, \ \nabla v_1 = \nabla v_2 \tag{5}$$

and in (4) iff

$$U_1 \cdot \nabla E = U_2 \cdot \nabla E. \tag{6}$$

From (5) we have

$$u_1 - u_2 = c_1, \qquad v_1 - v_2 = c_2 \tag{7}$$

where c_1 and c_2 are constants. From (6) we get

$$E_x(u_1 - u_2) + E_y(v_1 - v_2) = 0. \tag{8}$$

But as E_x and E_y are linearly independent, (7) and (8) gives

$$u_1 = u_2, \qquad v_1 = v_2,$$

which implies

$$U_1 = U_2.$$

Hence, for $U_1 \neq U_2$ we have,

$$\int_{\Omega} ((\alpha U_1 + (1-\alpha)U_2) \cdot \nabla E)^2 dxdy < \alpha \int_{\Omega} (U_1 \cdot \nabla E)^2 dxdy + (1-\alpha) \int_{\Omega} (U_2 \cdot \nabla E)^2 dxdy.$$

This gives,

$$J(\alpha U_1 + (1-\alpha)U_2) < \alpha J(U_1) + (1-\alpha)J(U_2), \qquad 0 < \alpha < 1. \tag{9}$$

Thus J is a strictly convex functional with respect to U.

Next, we state a result showing that the constraint set (2) is a closed subspace of Z, which can be proved by standard arguments (for e.g., see [30]).

Theorem 6 *The constraint set (2) given as* $C = \{U \in Z : \nabla \cdot U = 0\}$ *is a closed subspace of* Z*.*

Thus, J is a strict convex function defined on H and the constraint set (2) denoted as K is a closed subspace of Z. We now show that J is continuous and coercive.

Theorem 7 *The functional* J *as given in (1) is continuous*

Proof We will use the Theorem 3 to prove our statement. We assume

$$\|E\|_{W^{1,\infty}(\Omega)} \leq M.$$

As $0 \in Z$, we consider a neighbourhood of zero given as $N_1 = \{U : \|U\|_Z < 1\}$. Now

$$\begin{aligned}
|J(U)| &= \left| \frac{1}{2} \int_\Omega (U \cdot \nabla E + E_t)^2 \, dxdy + \frac{K}{2} \int_\Omega \left[\|\nabla u\|^2 + \|\nabla v\|^2 \right] dxdy \right| \\
&\leq \frac{1}{2} \int_\Omega (U \cdot \nabla E + E_t)^2 \, dxdy + \frac{K}{2} \|U\|_Z^2 \\
&\leq \frac{1}{2} \int_\Omega \left(E_t^2 + (U \cdot \nabla E)^2 + 2E_t (U \cdot \nabla E) \right) dxdy + \frac{K}{2} \|U\|_Z^2 .
\end{aligned}$$

Using Hölder's inequality and L^∞ bound on E and its derivatives, we get

$$\begin{aligned}
|J(U)| &\leq \frac{1}{2} \int_\Omega \left[M^2 + M^2 (u+v)^2 \right] dxdy \\
&\quad + 2M \left(\int_\Omega (\nabla E)^2 \right)^{1/2} \left(\int_\Omega U^2 \right)^{1/2} dxdy + \frac{K}{2} \|U\|_Z^2 \\
&\leq \frac{M^2}{2} \int_\Omega \left[1 + 2(u^2 + v^2) \right] dxdy + M\left(\int_\Omega M^2\right)^{1/2} \|U\|_Z + \frac{K}{2} \|U\|_Z^2 \\
&\leq \frac{M^2}{2} \left(\int_\Omega 1\right) + M^2 \|U\|_Z^2 + M^2 \left(\int_\Omega 1\right) + \frac{K}{2} \|U\|_Z^2 \\
&< \frac{3M}{2} \mu(\Omega) + M^2 + \frac{K}{2} \qquad (\text{ as } \|U\|_Z < 1) \\
&< \infty,
\end{aligned}$$

where $\mu(\Omega)$ is the measure of Ω. This gives us $J(U)$ is bounded above in N_1. As J is convex (by Theorem 5), it implies J is continuous for all $U \in Z$ (by Thoerem 3).

Theorem 8 *The functional J as given in (1) is coercive under the assumption that E_x and E_y are linearly independent.*

Proof The functional J in (1) can be written as

$$J(U) = J_1(U) + \int_\Omega \{E_t^2 + 2E_t (U \cdot \nabla E)\} dxdy$$

where,

$$J_1(U) = \int_\Omega (U \cdot \nabla E)^2 dxdy + \frac{K}{2} \int_\Omega \|\nabla U\|^2 dxdy. \tag{10}$$

To show $J(U)$ is coercive, we need to show $J_1(U)$ is coercive as it is quadratic in U. We use the Poincare-Wirtinger's Inequality

$$\int_\Omega (U - T)^2 dxdy \leq D \int_\Omega \|\nabla U\|^2 dxdy \tag{11}$$

where,

$$T = \frac{1}{\mu(\Omega)} \int_\Omega U dxdy \tag{12}$$

and D is a constant depending on Ω. Suppose, J_1 is not coercive. Then there does not exist any constant $M > 0$ such that

$$J_1(U) \geq M\|U\|_Z^2 \qquad \forall U \in Z$$

because if it was so then $J_1 \to \infty$ as $\|U\|_Z \to \infty$. So for any $M > 0$ there exists $U_M \in Z$ such that

$$J_1(U_M) < M\|U_M\|_Z^2.$$

We choose $M = \frac{1}{n}$ and get a sequence of M_n's and correspondingly get U_n. Without loss of generality, let us assume $\|U_n\|_Z = 1$. If not, we can take $V_n = \frac{U_n}{\|U_n\|_Z}$ and replace U_n with V_n. So we get a sequence $\{U_n\}_{n\in\mathbb{N}}$ in Z with $\|U_n\|_Z = 1$ and $J_1(U_n) \to 0$ as $n \to \infty$. Using (10) and (11) we have

$$\int_\Omega (u_n - T_n^1)^2 dxdy \to 0 \tag{13}$$

and

$$\int_\Omega (v_n - T_n^2)^2 dxdy \to 0 \qquad \text{for } n \to \infty, \tag{14}$$

where,

$$T_n^1 = \frac{1}{\mu(\Omega)} \int_\Omega u_n dxdy, \qquad T_n^2 = \frac{1}{\mu(\Omega)} \int_\Omega v_n dxdy.$$

As

$$\int_\Omega (E_x u + E_y v)^2 dxdy \leq 2|E_x^2|_\infty \int_\Omega u^2 dxdy + 2|E_y^2|_\infty \int_\Omega v^2 dxdy,$$

we have

$$\int_\Omega \left(E_x(u_n - T_n^1) + E_y(v_n - T_n^2)\right)^2 dxdy \to 0 \qquad \text{as } n \to \infty. \tag{15}$$

Now

$$\begin{aligned}
\left(\int_\Omega (E_x T_n^1 + E_y T_n^2)^2 dxdy\right)^{1/2} &= \left(\int_\Omega (E_x u_n + E_y v_n + E_x(T_n^1 - u_n) + E_y(T_n^2 - v_n))^2 dxdy\right)^{1/2} \\
&\leq \left(\int_\Omega (E_x u_n + E_y v_n)^2 dxdy\right)^{1/2} \\
&\quad + \left(\int_\Omega (E_x(T_n^1 - u_n) + E_y(T_n^2 - v_n))^2 dxdy\right)^{1/2} \\
&\leq (J_1(U_n))^{1/2} + \left(\int_\Omega (E_x(T_n^1 - u_n) + E_y(T_n^2 - v_n))^2 dxdy\right)^{1/2} \\
&\to 0 \text{ for } n \to \infty. \qquad \text{(Using (15))}
\end{aligned}$$

Let $a = E_x T_n^1, \quad b = E_y T_n^2$. Then,

$$\begin{aligned}
\|a+b\|_H^2 &= \|a\|_H^2 + \|b\|_H^2 + 2(a,b)_H \\
&\geq \|a\|_H^2 + \|b\|_H^2 - 2\|a\|_H\|b\|_H \frac{|(a,b)|_H}{\|a\|_H\|b\|_H} \\
&\geq \|a\|_H^2 + \|b\|_H^2 - (\|a\|_H^2 + \|b\|_H^2)\frac{|(a,b)|_H}{\|a\|_H\|b\|_H} \\
&= (\|a\|_H^2 + \|b\|_H^2)\{1 - \frac{|(a,b)|_H}{\|a\|_H\|b\|_H}\},
\end{aligned}$$

where $(a,b)_H$ is the usual inner product in H. Thus we get

$$\int_\Omega (E_x T_n^1 + E_y T_n^2)^2 dxdy \geq \left(\|E_x\|_H^2 (T_n^1)^2 + \|E_y\|_H^2 (T_n^2)^2\right)\{1 - \frac{|(E_x,E_y)|_H}{\|E_x\|_H\|E_y\|_H}\}. \tag{16}$$

As left hand side of (16) $\to 0$ as $n \to \infty$ and by linear independency of E_x and E_y,

$$1 - \frac{|(E_x,E_y)|_H}{\|E_x\|_H\|E_y\|_H} > 0$$

and since $\|E_x\|_H$ and $\|E_y\|_H$ are not identically 0, we have

$$T_n^1 \to 0 \text{ and } T_n^2 \to 0 \text{ as } n \to \infty. \tag{17}$$

But this gives a contradiction as $\|U_n\|_Z \leq \|(U_n - T_n)\|_Z + \|T_n\|_Z$ and hence $\|U_n\|_Z \to 0$ as $n \to \infty$ (using (13),(14),(17)). So J_1 is coercive and hence J is coercive.

By Thoerem 4, the problem (P) has an unique global minimum.

4 Exact recovery of Stokes flow

We now write down the optimality conditions for the minimizer of (P). Using Lagrange multipliers, the auxillary functional can be written as

$$\widetilde{J}(U,p) = \frac{1}{2}\int_\Omega (E_t + U \cdot \nabla E)^2 \, dxdy + \frac{K}{2}\int_\Omega \|\nabla U\|^2 \, dxdy + \int_\Omega (\nabla \cdot U)p \, dxdy$$

Taking Gateaux derivative of $\widetilde{J}$ with respect to U and p, the standard optimality conditions [23] are

$$\frac{\partial \widetilde{J}}{\partial U} = 0 \quad \text{and} \quad \frac{\partial \widetilde{J}}{\partial p} = 0. \tag{18}$$

The first equation in (18) gives

$$\int_{\Omega}(E_t + (U\cdot\nabla E))(\overline{U}\cdot\nabla E) + K\int_{\Omega}(\nabla u\cdot\nabla\overline{u}) + (\nabla v\cdot\nabla\overline{v}) + \int_{\Omega}(\nabla\cdot\overline{U})p = 0, \quad \forall\,\overline{U}\in Z \tag{19}$$

with prescribed Dirichlet boundary conditions

$$U = U_b \qquad \text{on} \ \ \partial\Omega. \tag{20}$$

The second equation in (18) gives

$$\int_{\Omega}(\nabla\cdot U)\overline{p} = 0, \qquad \forall\overline{p}\in L^2(\Omega). \tag{21}$$

Let

$$Z_b = \{U\in Z : U = U_b \text{ on } \partial\Omega\}. \tag{22}$$

Performing an integration by parts on the second term on the left in (19) and taking $\overline{U}$ to be an arbitrary function in Z, together with (21), the following PDE is obtained

$$\begin{aligned} K\Delta U - \nabla p &= -(E_t + U\cdot\nabla E)\nabla E \\ \nabla\cdot U &= 0 \end{aligned} \tag{23}$$

subject to (20), where $(U,p)\in(Z\cap Z_b)\times(L^2(\Omega)\setminus\mathbb{R})$.

Remark 1 We use the space for pressure as $L^2(\Omega)\setminus\mathbb{R}$ so that in the discrete formulation we can look for a pressure whose value is specified at a point. [31, Remark 9.1.1]

Theorem 9 *Let E in the right hand side of (23) be advected with velocity U_e i.e.,*

$$E_t + U_e\cdot\nabla E = 0$$

with U_e satisfying (20) and incompressible Stokes equation

$$\begin{aligned} &\alpha\Delta U_e + \nabla q = f, \qquad \alpha > 0 \\ &\nabla\cdot U_e = 0. \end{aligned} \tag{24}$$

If f is given by a potential $f = \nabla\phi$ for smooth ϕ, then $U = U_e$ is the only solution of (23), which is independent of any $K > 0$. In other words, the flow is recovered exactly irrespective of K.

Proof Eq. (23) can rewritten as

$$\alpha\Delta U - \frac{\alpha}{K}\nabla p = -\frac{\alpha}{K}(E_t + U\cdot\nabla E)\nabla E \tag{25}$$

Since $f = \nabla\phi$, Eq. (24) can be rewritten as

$$\alpha\Delta U_e + \nabla(q+\phi) = 0.$$

As the image E is advected with velocity, U_e is a solution of Eq. (25) with $p = -\frac{K}{\alpha}(q+\phi)$ and right hand side as zero. As the solution of (23) is unique, $U = U_e$ is the unique solution of (23), which is independent of any $K > 0$.

The result of Theorem 9 is verified in the numerical examples in Section 6 where we have considered incompressible Stokes flow under various boundary conditions and find that the flow is recovered with a high precision. Also as Navier-Stokes flow at low Reynolds number represents Stokes flow, we recover low Reynolds number Navier-Stokes flow exactly.

5 Finite element method for the Optical flow problem (1)

Eq. (23) is solved using the finite element method. Combining equations (19) and (21) along with the boundary conditions (20) gives the weak formulation of the PDE to be solved to determine the minimizer. Let T_h be a triangulation of domain Ω and let K be a triangle in T_h. Let Z_h and X_h be two finite element spaces with triangulation parameter h such that

$$Z_h \subset Z, \qquad X_h \subset L^2(\Omega).$$

Then the discrete problem is to find $(U_h, p_h) \in (Z_h \cap Z_b) \times X_h$ such that

$$\begin{gathered}\int_\Omega (E_t + (U_h \cdot \nabla E))(\nabla E \cdot \overline{U}_h) + K \int_\Omega (\nabla u_h \cdot \nabla \overline{u}_h) + (\nabla v_h \cdot \nabla \overline{v}_h) + \int_\Omega (\nabla \cdot \overline{U}_h) p_h = 0 \\ \int_\Omega (\nabla \cdot U_h) \overline{p}_h = 0\end{gathered} \tag{26}$$

where, $(\overline{U}_h, \overline{p}_h) \in Z_h \times X_h$.
Let us define the following Taylor-Hood finite element spaces

$$Z_h(\Omega) = \{U_h \in (C^0(\Omega))^2 : U_h|_K \text{ is a polynomial of degree 2 and } U_h = 0 \text{ on } \partial\Omega\} \tag{27}$$

and

$$X_h(\Omega) = \{p_h \in C^0(\Omega) : p_h|_K \text{ is a polynomial of degree 1}\}, \tag{28}$$

which satisfy the LBB condition [22]. Using this condition, one can show that there exists an unique solution $(U_h, p_h) \in (Z_h \cap Z_b) \times X_h$ [31, Eq. 9.2.10]. We now describe the procedure to determine E, E_t and ∇E.

5.1 Image data

Our aim is to generate a sequence of synthetic images E and try to recover the velocity given the information of the derivatives of E. For this purpose E is chosen whose analytic expression is known at time $t = 0$ and hence its gradients can be computed exactly. To advect E with velocity U_e exactly, E_t at $t = 0$ is generated from the equation

$$E_t(x, y, 0) = -U_e \cdot \nabla E(x, y, 0)$$

where U_e represents the velocity obtained by solving incompressible Stokes flow

$$\begin{aligned} \Delta U + \nabla p &= f \\ \nabla \cdot U &= 0, \end{aligned} \tag{29}$$

or Navier-Stokes flow

$$\begin{aligned} -\alpha \Delta U + (U \cdot \nabla) U + \nabla p &= f, \\ \nabla \cdot U &= 0, \end{aligned} \tag{30}$$

using finite element method with appropriate boundary conditions, where $\alpha = 1/Re$ and Re is the Reynolds number. In practice, derivatives of images will be computed using some finite differences which will introduce errors in the computed velocity.

5.2 Test Flows

Two types of flows are considered: one in a lid-driven cavity and the other past a cylinder. For flows in a lid-driven cavity, the domain is $\Omega = [0, 1] \times [0, 1]$. The boundary conditions are

$$U = \begin{cases} (1, 0) & \text{on } y = 1 \\ (0, 0) & \text{elsewhere} \end{cases} \tag{31}$$

with image at time t_0 defined as

$$E_0(x, y) = E(x, y, 0) = e^{-50[(x-1/2)^2 + (y-1/2)^2]}.$$

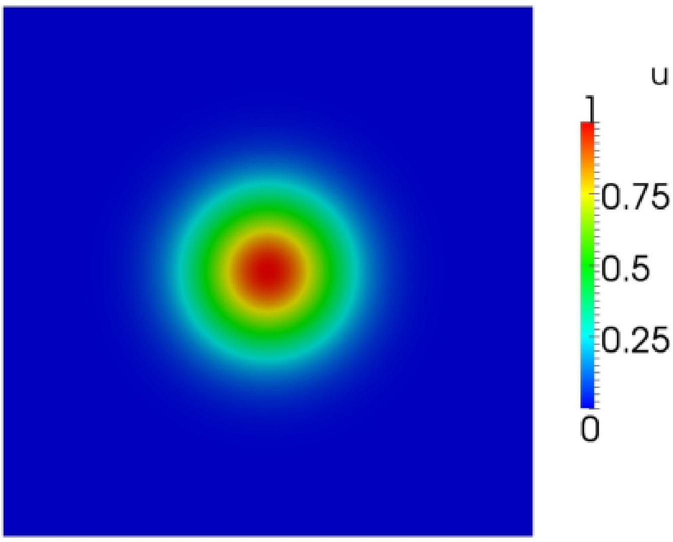

Fig. 1: Image at time $t = 0$

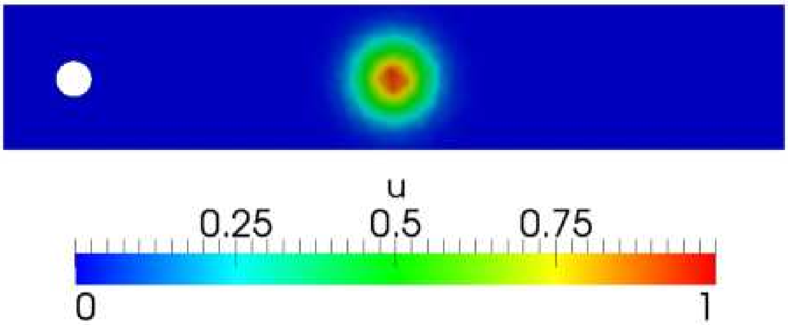

Fig. 2: Image at time $t = 0$

For flows past a cylinder, the domain Ω is a rectangle in $\mathbb{R}^2$ given as $[0, 2.2] \times [0, 0.41]$ with a closed disk inside it centered at $(0.2, 0.2)$ and radius 0.05. The boundary conditions are

$$U = \begin{cases} (0,0) & \text{on } y = 0, y = 0.41 \text{ and on the surface of the disk} \\ (0, \frac{6y(0.41-y)}{0.41^2}) & \text{on } x = 0 \end{cases} \tag{32}$$

with image at time t_0 defined as

$$E_0(x,y) = E(x,y,0) = e^{-50[(x-1.1)^2+(y-0.2)^2]}.$$

To compute U_e, Eq. (29) or (30) is solved subject to the boundary conditions given in (31) or (32). But exact analytic expressions of solutions to (29) or (30) with the specified boundary conditions are usually not known. Thus finite element method is used to obtain U_e.

5.3 Mesh

For flows in a lid-driven cavity, the domain $\Omega = [0,1] \times [0,1]$ is triangulated with 100 points on each side as shown in Figure 3. There are 20000 triangles with 10201 degrees of freedom. For flows past a cylinder, the mesh used is shown in Figure 4. It comprises of 200 points on the longer boundary, 80 points on the shorter boundary and 100 points on the circular boundary. There are 28582 triangles with 14605 degrees of freedom.

5.4 Solving the Stokes equation

To solve (29), let us write the weak formulation as: find $U \in Z_b$ defined in (22) and $p \in L^2(\Omega) \setminus \mathbb{R}$ such that

$$\int_\Omega \nabla U \cdot \nabla V + \int_\Omega (\nabla \cdot V)p + \int_\Omega (\nabla \cdot U)q + \int_\Omega f \cdot V = 0, \qquad \forall (V,q) \in Z \times L^2(\Omega). \tag{33}$$

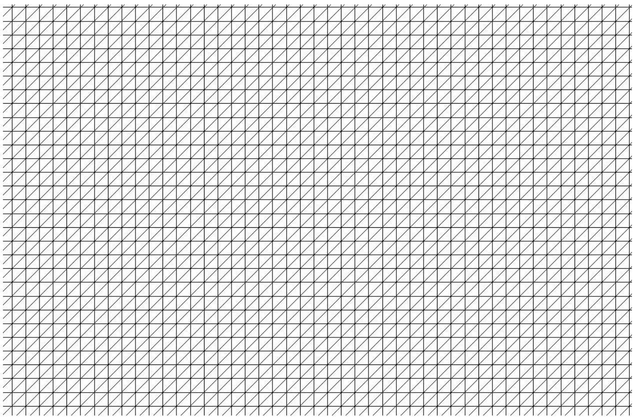

Fig. 3: Zoomed view of mesh for the lid-driven cavity flows.

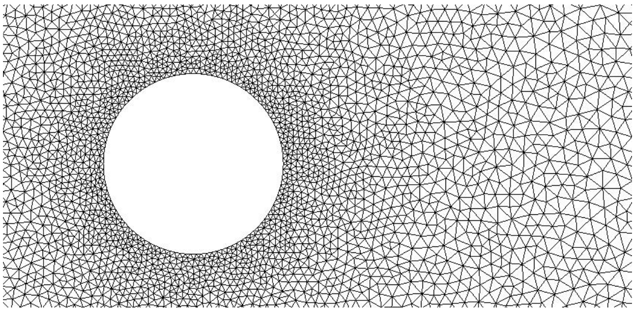

Fig. 4: Zoomed view of mesh for the lid-driven cavity flows.

We also fix the value of p to be zero at a point $X_0 \in \partial\Omega$ to obtain uniqueness thus being consistent with the space for pressure (see Remark 1). The discrete problem is to find $(U_h, p_h) \in (Z_h \cap Z_b) \times X_h$ such that

$$\int_\Omega \nabla U_h \cdot \nabla V_h - \int_\Omega (\nabla \cdot V_h) p_h - \int_\Omega (\nabla \cdot U_h) q_h = \int_\Omega f \cdot V_h, \qquad \forall (V_h, q_h) \in Z_h \times X_h, \tag{34}$$

where Z_h and X_h are defined in (27) and (28) respectively. Solving Eq. (34) with domains, boundary conditions and meshes defined in Sections 5.2 and 5.3 gives U_e.

5.5 Solving the Navier-Stokes equation

Eq. (30) is a non-linear equation in U. The method of Picard iteration, which is an easy way of handling nonlinear PDEs, is thus used. In this method, a previous solution in the nonlinear terms is used so that these terms become linear in the unknown U. The strategy is also known as the method of successive substitutions [21]. In our case, we seek a new solution U^{k+1} in iteration $k+1$ such that (U^{k+1}, p^{k+1}) solves the linear problem

$$\begin{aligned} -\alpha \Delta U^{k+1} + (U^k \cdot \nabla)U^{k+1} + \nabla p^{k+1} &= f, \\ \nabla \cdot U^{k+1} &= 0 \end{aligned} \tag{35}$$

with given boundary conditions, where U^k is known. The variational formulation for (35) can be written as: find $U^{k+1} \in Z_b = \{U \in Z : U = U_b \text{ on } \partial\Omega\}$ and $p^{k+1} \in L^2(\Omega) \setminus \mathbb{R}$ such that

$$\begin{aligned} \int_\Omega \alpha \nabla U^{k+1} \cdot \nabla V + \int_\Omega \left[(U^k \cdot \nabla)U^{k+1}\right] \cdot V - \int_\Omega (\nabla \cdot V) p^{k+1} - \int_\Omega (\nabla \cdot U^{k+1}) q \\ - \int_\Omega f \cdot V = 0, \quad \forall (V, q) \in Z \times L^2(\Omega). \end{aligned} \tag{36}$$

We start with initial guess $U^0 = (0, 0)$ and employ the finite element method as described in Section (5.4) to determine U^{k+1}. Finally, we stop at the $k+1^{th}$ stage if $\|U^{k+1} - U^k\| < \epsilon$. We choose $\epsilon = 10^{-7}$. Hence we have $U_e = U^{k+1}$. The convergence of the fixed point iteration method (36) has been shown in [32, Sec 6.3].
Finally, the relative L^2 error in velocity is defined as

$$\text{Relative } L^2 \text{ error} = \frac{\|U_e - U_o\|}{\|U_e\|} \tag{37}$$

and the advection error is defined as

$$\text{Advection Error} = \|E_t + U_o \cdot \nabla E\| \tag{38}$$

where U_e is the exact velocity and U_o is the obtained velocity and the norm $\|\cdot\|$ is the usual L^2 norm for vector functions as defined earlier.

6 Numerical Examples

6.1 Stokes Flow in a lid driven cavity

The exact flow is given by solving (29) with $f = (1, 100)$ in lid-driven cavity. Figure (5) shows plots of velocity vectors for various K. The velocity is recovered with a very high degree of accuracy. This is also reflected in the relative L^2 errors given in Table (1). Also, Table (1) shows that the advection errors are very small and so the recovered velocity preserves the advection properties of the image. The streamline plots for the velocity given in Figures (6) show that large vortex in the center and the two small vortices at the bottom corners are detected with good accuracy, which is actually very important in atmospheric flows. It is notable that the regularization parameter K has minimal effect on the behaviour of the solutions, which is consistent with the fact that it is

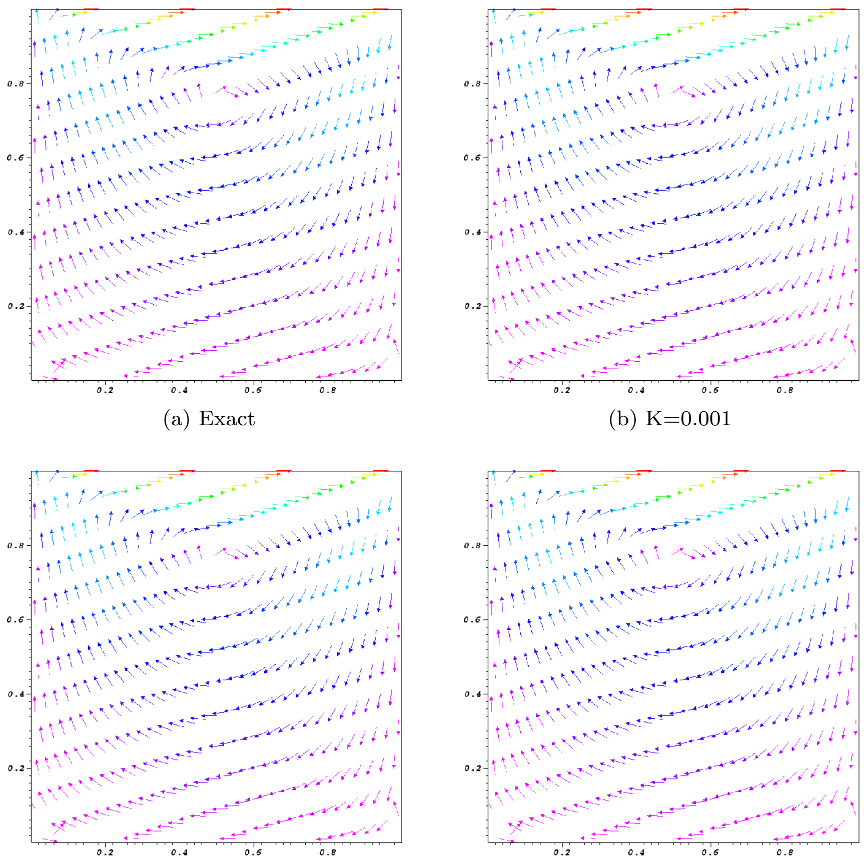

(a) Exact

(b) K=0.001

(c) K=5

(d) K=35

Fig. 5: Velocity plots for Stokes flow in a lid driven cavity

K	Relative L^2 Error	Advection Error
0.001	4.55e-08	9.62e-26
5	4.56e-08	6.83e-27
110	4.49e-08	2.51e-27
300	4.48e-08	4.11e-27
600	4.42e-08	3.57e-28

Table 1: Variation of relative L^2 error and advection error with K for Stokes flow in a lid driven cavity

not a physical parameter and hence, any positive value of K can be used to determine the velocity. This perfectly justifies the result proved in Theorem 9.

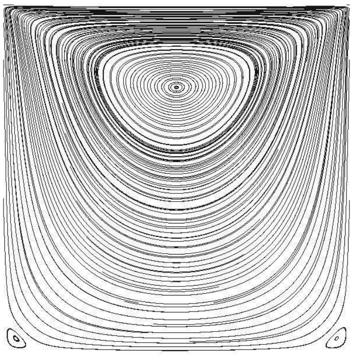

(a) Exact

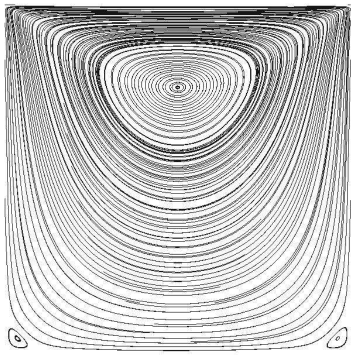

(b) K=0.001

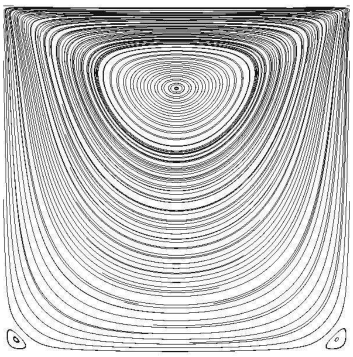

(c) K=5

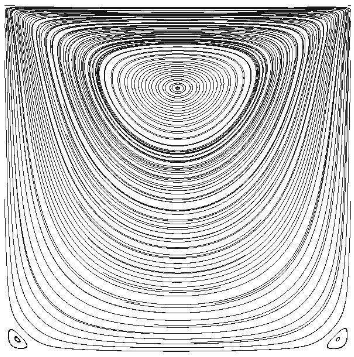

(d) K=35

Fig. 6: Streamline plots for Stokes flow in a lid driven cavity

6.2 Stokes flow past a cylinder

The exact flow is given by solving (29) as a flow past a cylinder with $f = (1, 100)$. Figure (7) shows plots of velocity vectors for various K. Again the velocity is recovered with a very high degree of accuracy. Table (2) shows the relative L^2 errors and the advection errors, which are quite small, justifying good recovery of flows. The streamline plots for the velocity is given in Figure (8). As with the case of Stokes flow in a lid driven cavity, there is no dependence of the obtained solutions on K.

6.3 Navier-Stokes flow in a lid driven cavity for $Re = 1$ and 1000

Here we consider motion governed by Navier-Stokes flows for $Re = 1$ and 1000. The exact flow is given by solving (30) with $f = (1, 100)$ in a lid-driven cavity. Figures (9) and (11) show the velcity vector plots for $Re = 1$ and $Re = 1000$

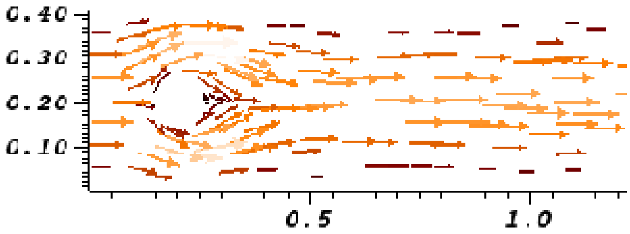

(a) Exact

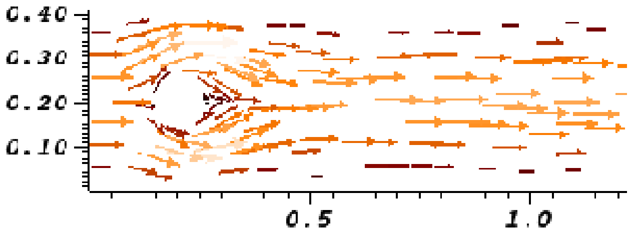

(b) K=0.001

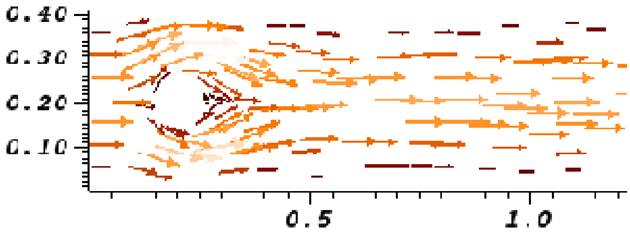

(c) K=5

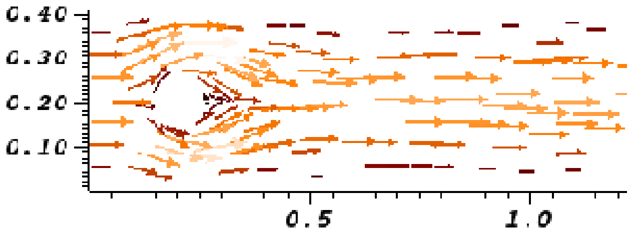

(d) K=35

Fig. 7: Velocity plots for Stokes flow past a cylinder

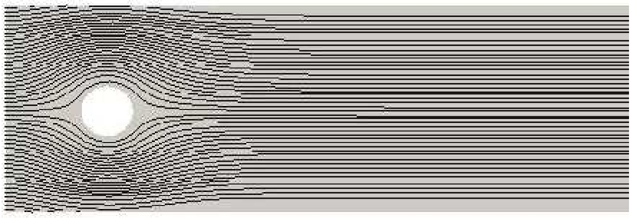

(a) Exact

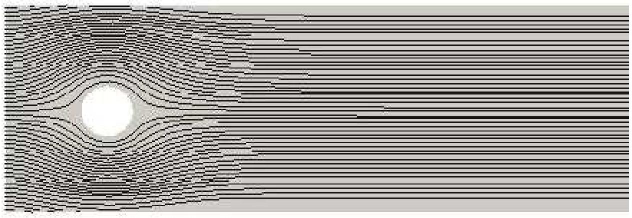

(b) K=0.001

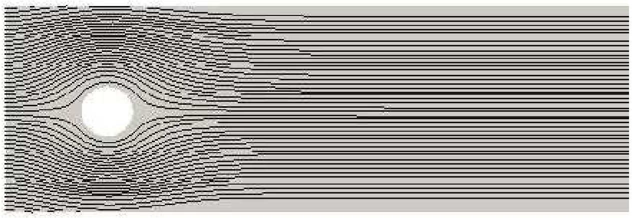

(c) K=5

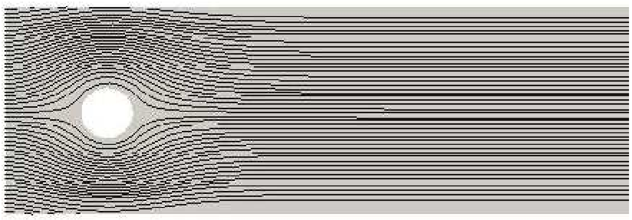

(d) K=35

Fig. 8: Streamline plots for Stokes flow past a cylinder

K	Relative L^2 Error	Advection Error
0.001	1.44e-8	3.76e-28
5	1.53e-8	6.43e-27
110	1.47e-8	6.69e-28
300	1.42e-8	5.25e-28
600	1.69e-8	5.32e-28

Table 2: Variation of relative L^2 error and advection error with K for Stokes flow past a cylinder

K	Relative L^2 Error	Advection Error
0.001	3.56e-4	2.7e-11
5	3.61e-4	2.8e-11
110	3.44e-4	3.1e-11
300	3.48e-4	2.9e-11
600	3.4e-4	2.6e-11

Table 3: Variation of relative L^2 error and advection error with K for Navier-Stokes flow in a lid driven cavity for $Re = 1$

K	Relative L^2 Error	Advection Error
0.001	5.81e-1	2.8e-8
5	5.95e-1	3.6e-8
110	6.12e-1	4.1e-8
300	6.07e-1	2.5e-8
600	5.86e-1	5.2e-8

Table 4: Variation of relative L^2 error and advection error with K for Navier-Stokes flow in a lid driven cavity for $Re = 1000$

respectively. The plots show good recovery for $Re = 1$, whereas for $Re = 1000$ the relative L^2 error is on the higher side. This is also reflected in Tables (3) and (4). The streamline plots given by Figures (10), (12) show that for lower Reynolds number flows the vortices are well recovered whereas for higher Reynolds number flows the vortices are recovered though not to a greater degree of accuracy. Tables (3) and (4) suggests that the advection error for lower Reynolds number flows is very low compared to higher Reynolds number flows. This is because at low Reynolds number, Navier-Stokes flows represents Stokes flows and hence they are recovered well. For higher Reynolds number flows, the non-linear convection term dominates and so a very good flow recovery is not possible with our linear model. However, we note that even for higher Reynolds number flows, the solution obtained is independent of K.

6.4 Navier-Stokes flow past a cylinder.

The exact flow is given by solving (30) as a flow past a cylinder with $f = (1, 100)$. Figures (13) and (15) show the velocity vector plots for $Re = 1$ and

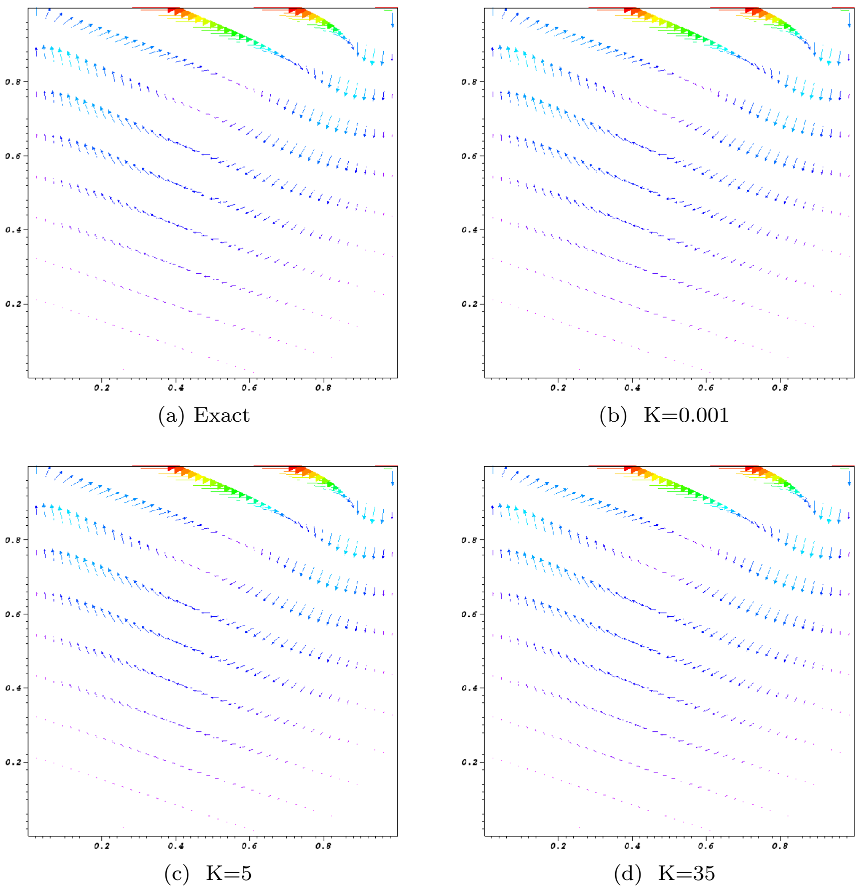

(a) Exact (b) K=0.001

(c) K=5 (d) K=35

Fig. 9: Velocity plots for Navier-Stokes flow in a lid driven cavity for $Re = 1$

$Re = 1000$ respectively. The plots show good recovery for $Re = 1$, whereas for $Re = 1000$ the relative L^2 error is on the higher side, which is also reflected in Tables (5) and (6). The streamline plots given by Figures (14) and (16) show that vortices for low Reynolds number flows are captured well whereas for higher Reynolds number flows, the vortices behind the cylinder are not captured. This suggests there is a need to include extra assumptions in our model for high Reynolds number flows.

7 Conclusion

A variational technique for tracking instantaneous motion from flow images using the well-known OFM has been formulated. In the present work, these flow images have been generated by numerically solving the 2D incompressible Stokes equation (29) or the Navier-Stokes equations (30) for $Re = 1$ and 1000.

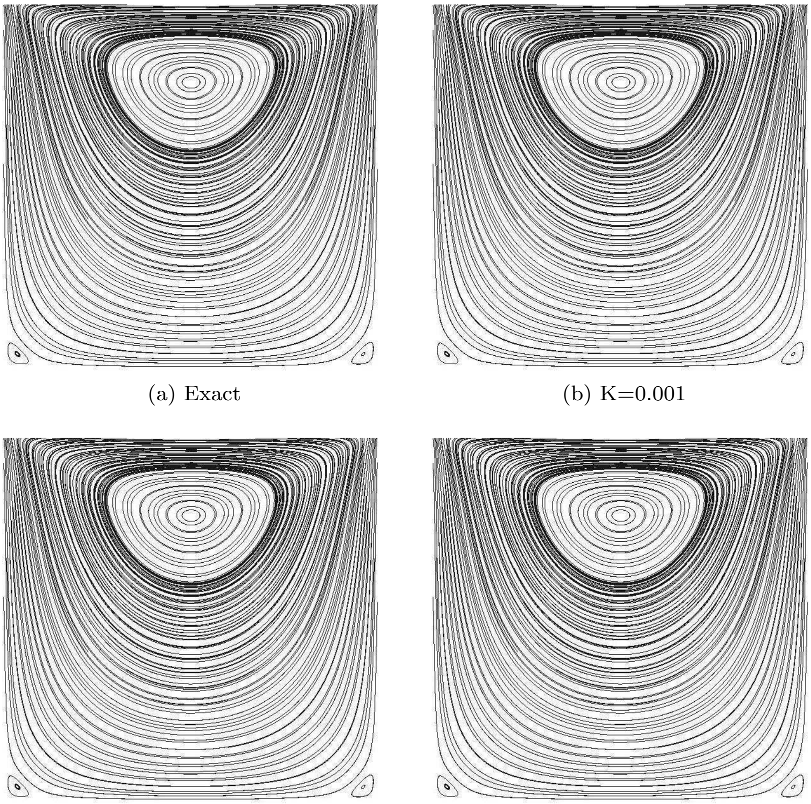

(a) Exact

(b) K=0.001

(c) K=5

(d) K=35

Fig. 10: Streamline plots for Navier-Stokes flow in a lid driven cavity for $Re = 1$

K	Relative L^2 Error	Advection Error
0.001	1.01e-4	2.0e-11
5	1.11e-4	2.0e-11
110	1.24e-4	2.1e-11
300	1.15e-4	2.5e-11
600	1.08e-4	2.6e-11

Table 5: Variation of relative L^2 error and advection error with K for Navier-Stokes flow past a cylinder for $Re = 1$

Incompressibility is the only constraint imposed in the variational formulation. Using FEM in the present variational approach method, it is shown that the velocities are recovered almost exactly for Stokes flow forced by potential. For Navier-Stokes flow the method performs very well for $Re = 1$ compared to $Re = 1000$. This is because Stokes flow is a linearized version of the Navier-Stokes flow for low Reynolds number. But nevertheless, in both the cases the physical features of fluid flow like vortex structures are captured well. This

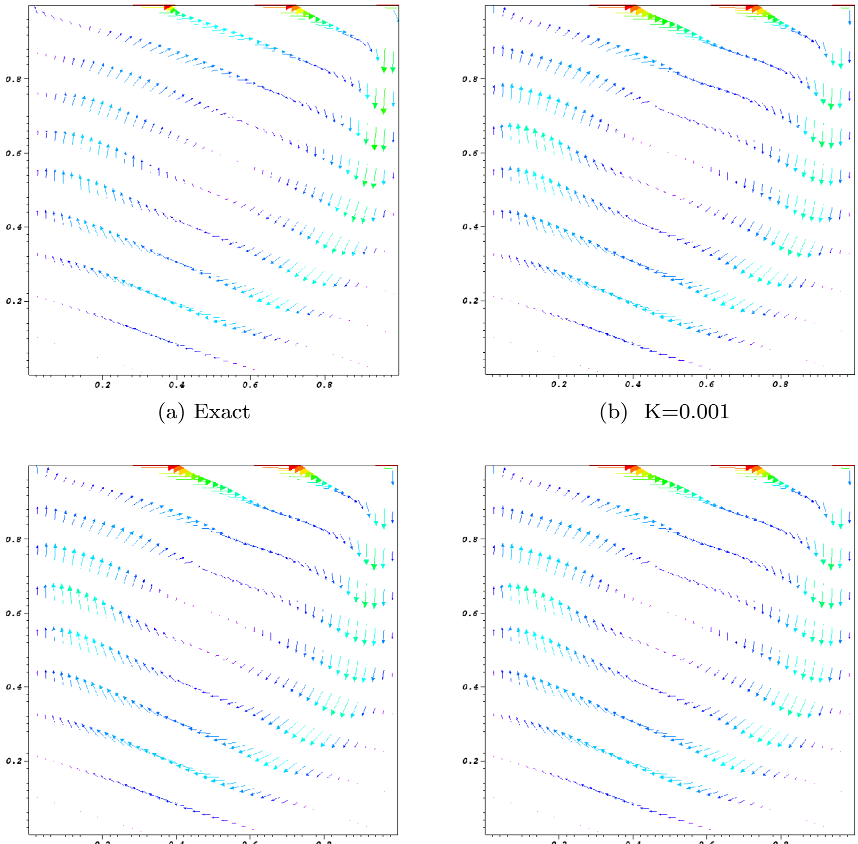

(a) Exact (b) K=0.001

(c) K=5 (d) K=35

Fig. 11: Velocity plots for Navier-Stokes flow in a lid driven cavity for $Re = 1000$

K	Relative L^2 Error	Advection Error
0.001	7.23e-1	4.3e-8
5	6.56e-1	4.6e-8
110	6.12e-1	4.6e-8
300	6.33e-1	4.5e-8
600	6.86e-1	4.7e-8

Table 6: Variation of relative L^2 error and advection error with K for Navier-Stokes flow past a cylinder for $Re = 1000$

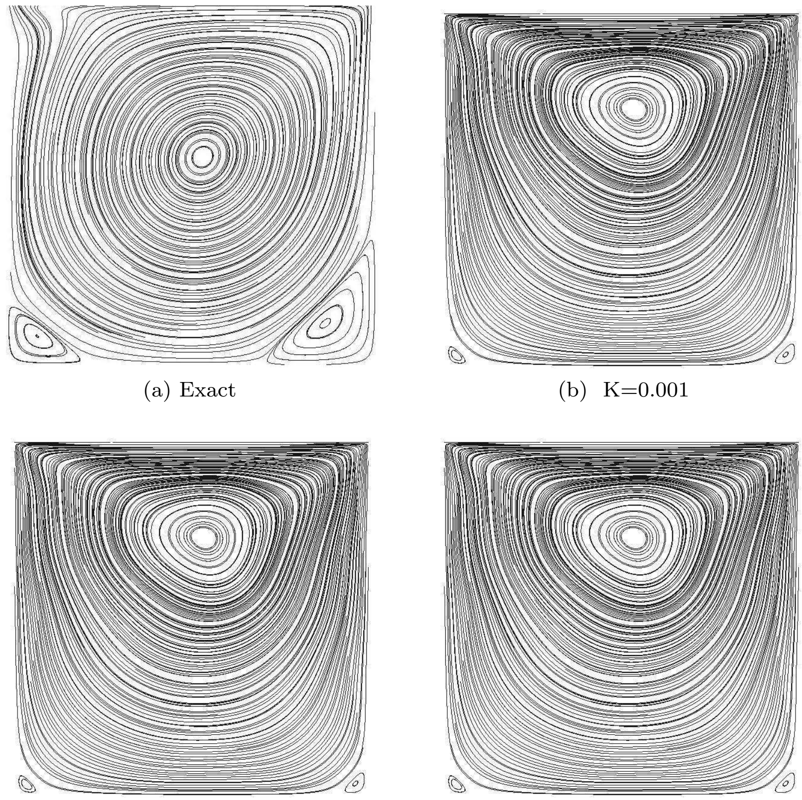

(a) Exact (b) K=0.001

(c) K=5 (d) K=35

Fig. 12: Streamline plots for Navier-Stokes flow in a lid driven cavity for $Re = 1000$

is particularly attractive for the cloud motion problem. The simplicity of our variational approach makes it computationally attractive. In future, we plan to extend this variational approach to track high Reynolds number flows as well.

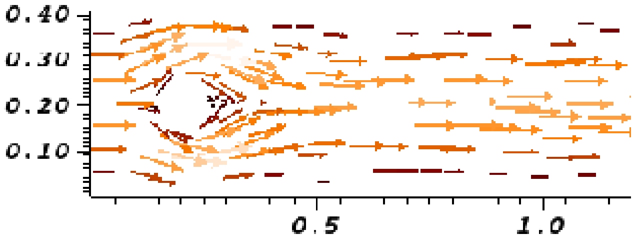

(a) Exact

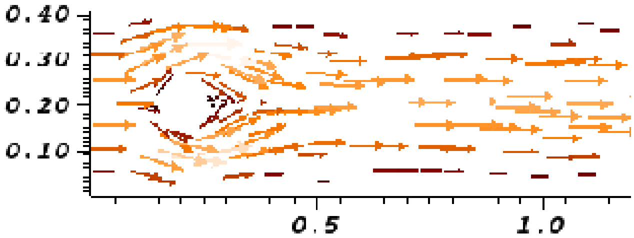

(b) K=0.001

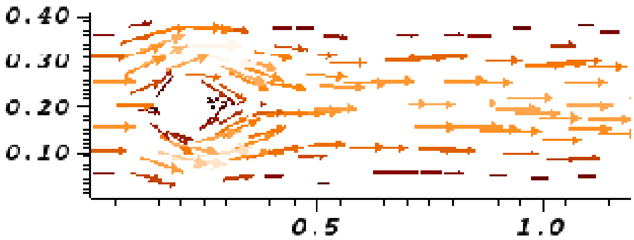

(c) K=5

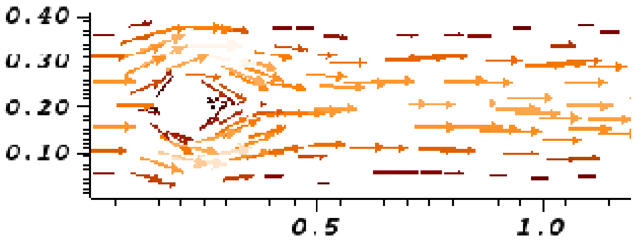

(d) K=35

Fig. 13: Velocity plots for Navier-Stokes flow past a cylinder for $Re = 1$

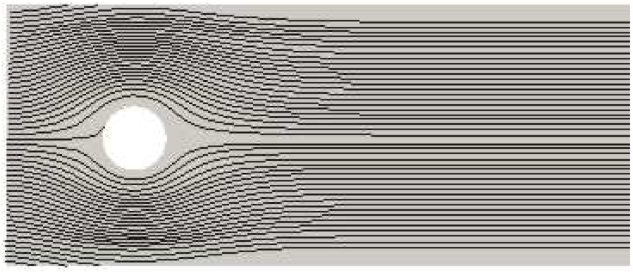

(a) Exact

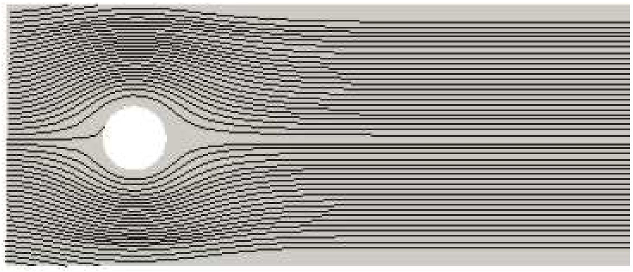

(b) K=0.001

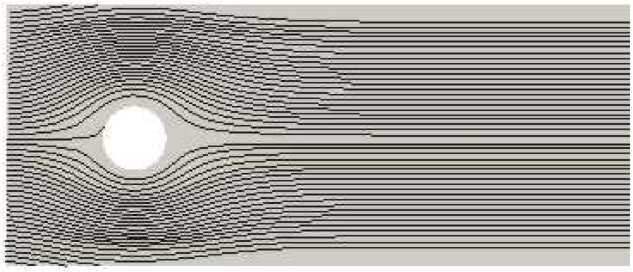

(c) K=5

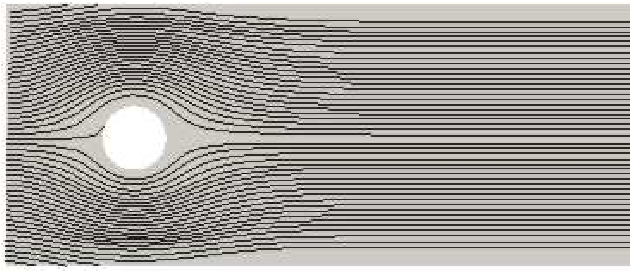

(d) K=35

Fig. 14: Streamline plots for Navier-Stokes flow past a cylinder for $Re = 1$

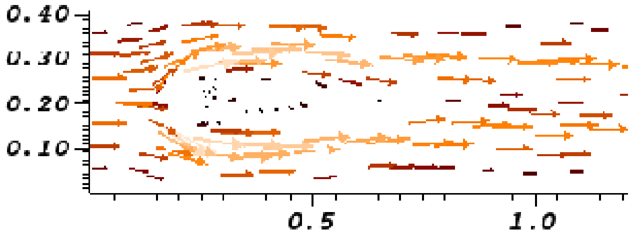

(a) Exact

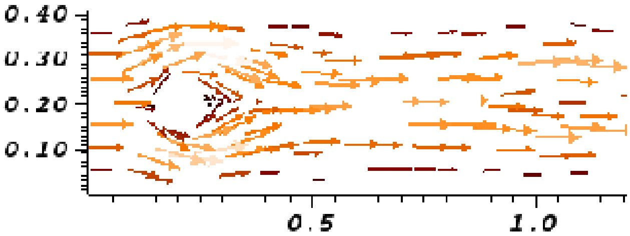

(b) K=0.001

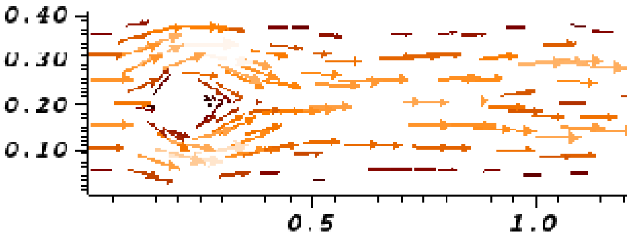

(c) K=5

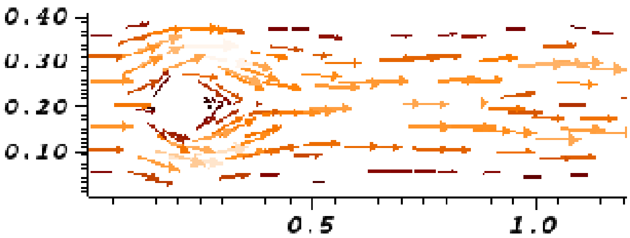

(d) K=35

Fig. 15: Velocity plots for Navier-Stokes flow past a cylinder for $Re = 1000$

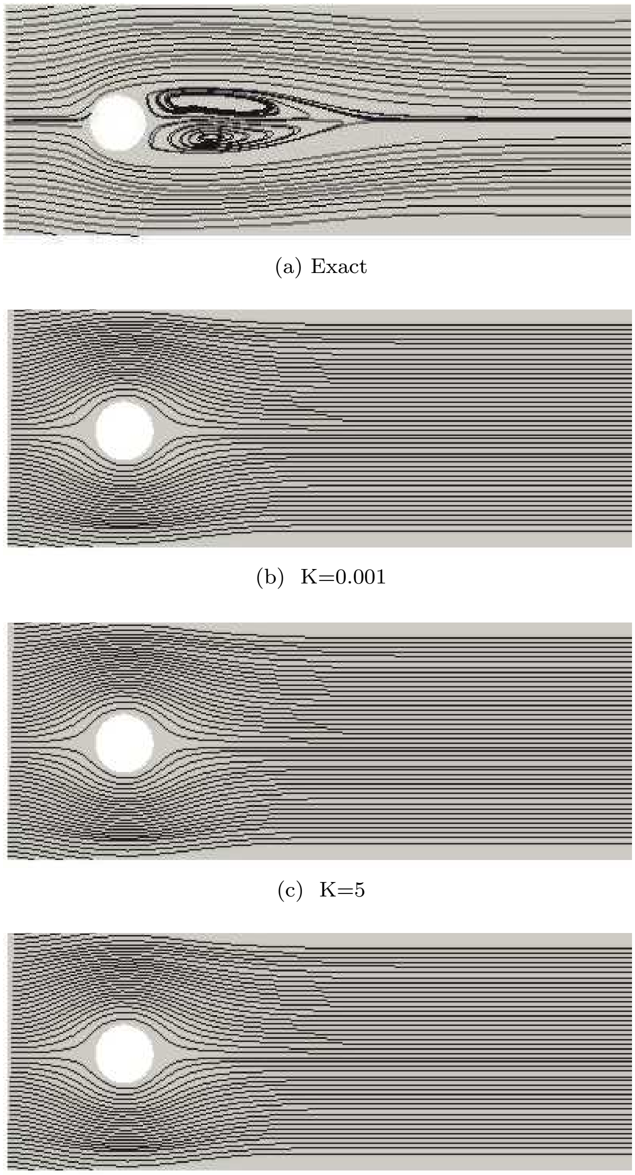

(a) Exact

(b) K=0.001

(c) K=5

(d) K=35

Fig. 16: Streamline plots for Navier-Stokes flow past a cylinder for $Re = 1000$

References

1. Cayula, J.–F. and Cornillon, P. Cloud detection from a sequence of SST images. *Remote Sens. Env.*, 55(1996)80–88.
2. Leese, J. A., Novak, C. S. and Taylor, V. R. The determination of cloud pattern motions from geosynchronous satellite image data. *Pattern Recog.*, 2(1970) 279–292.
3. Fogel, S. V. The estimation of velocity vector-fields from time varying image sequences. *CVGIP: Image Understanding*, 53(1991) 253–287.
4. Wu, Q. X. A correlation-relaxation labeling framework for computing optical flow-Template matching from a new perspective. *IEEE Trans. Pattern Analysis and Machine Intelligence*, 17(1995) 843–853.
5. Parikh, J. A., DaPonte, J. S., Vitale, J. N. and Tselioudis, G. An evolutionary system for recognition and tracking of synoptic scale storm systems. *Pattern Recognition Letters*, 20(1999) 1389–1396.
6. Liu, T. and Shen, L. Fluid Flow and optical flow. *J. Fluid Mech*, 614(2008) 253–291.
7. Horn, B. K. P. and Schunck, B. G. Determining optical flow. *Artificial Intelligence*, 17(1-3)(1981) 185–203.
8. Ruhnau, P. and Schnörr, C. Optical Stokes flow: An imaging based control approach. *Exp. Fluids*, 42(2007) 61–78.
9. Yuan, J., Ruhnau, P., Mémin, E., and Schnörr, C. Discrete orthogonal decomposition and variational fluid flow estimation. In *Scale-Space*, volume 3459(2005) of *Lect. Not. Comp. Sci.*, pages 267–278. Springer.
10. Heitz, D., Mémin, E. and Schnörr, C. Variational fluid flow measurement from image sequences: synopsis and perspectives. *Exp. Fluids*, 48(2010) 369–393.
11. Haussecker, H. W. and Fleet, D. J. Computing Optical Flow with Physical Models of Brightness Variation, *IEEE Transactions on Pattern Analysis and Machine Intelligence* , 23(6)(2001) 661–673.
12. Nagel, H.–H. On a constraint equation for the estimation of displacement rates in image sequences. *IEEE Trans. PAMI*, 11(1989) 13-30.
13. Papadakis, N. and Mémin, E. Variational assimilation of fluid motion from image sequence. *SIAM Journal on Imaging Sciences*, 1(4)(2008) 343-363.
14. Corpetti, T., Mémin, E., and Pérez, P. Dense estimation of fluid flows. *IEEE Trans. Pattern Anal. Mach. Intell.*, 24(3)(2002) 365–380.
15. Mukawa, N. Estimation of shape, reflection coefficients and illuminant direction from image sequences. *In ICCV90*, 1990, 507–512.
16. Nakajima, Y., Inomata, H., Nogawa, H., Sato, Y., Tamura, S., Okazaki, K. and Torii, S.. Physics-based flow estimation of fluids. *Pattern Recognition*, 36(5)(2003) 1203–1212.
17. Arnaud, E., Mémin, E., Sosa, R. and Artana, G. A fluid motion estimator for schlieren image velocimetry. *In ECCV06*, I(2006) 198–210.
18. Logg, A., Mardal, K.–A., Wells, G. N. Automated Solution of Differential Equations by the Finite Element Method. *Springer*, 2012.
19. Roy, S. Optical Flows - Determination of 2-D velocities of a moving fluid. *M.Phil Thesis, Tata Institute of Fundamental Research, CAM, Bangalore*, 2011.
20. Bauschke, H. H. and Combettes, P. L. Convex analysis and monotone operator theory in Hilbert spaces. *CMS Books in Mathematics, Springer* xvi+468 pp. ISBN: 978-1-4419-9466-0, 2011.
21. Langtengen, H. P. Computational Partial Differential Equations–Numerical methods and Diffpack programming. *Texts in Computational Science and Engineering, Springer* LII, 860 pp. ISBN: 978-3-642-55769-9, 2003.
22. Girault, V. and Raviart, P.–A. Finite Element Methods for Navier-Stokes Equations. Theory and Algorithms. *Springer Series in Computational Mathematics. Springer-Verlag*, Berlin, Germany, 1986.
23. Tröltzsch, F. Optimal Control of Partial Differential Equations: Theory, Methods and Applications. *Graduate Studies in Mathematics, American Mathematical Society*, Vol-112, 2010.
24. Aubert, G. and Kornprobst, P. A mathematical study of the relaxed optical flow problem in the space, *SIAM Journal of Math. Anal*, 30(6)(1999) 1282–1308.

25. Aubert, G., Deriche, R. and Kornprobst, P. Computing Optical Flow via Variational Techniques, *SIAM Journal of Math. Anal*, 60(1)(1999) 156-182.
26. Nagel, H.–H. Displacement vectors derived from second-order intensity variations in image sequences. *CGIP*, 21(1983) 85-117.
27. Nagel, H.–H. On the estimation of optical flow: Relations between different approaches and some new results. *AI*, 33(1987) 299-324.
28. Nagel, H.–H. and Enkelmann, W. An investigation of smoothness constraints for the estimation of displacement vector fields from image sequences. *IEEE Trans. PAMI*, 8(1986) 565-593.
29. Wayne Roberts, A. and Varberg, D. E. Convex Functions, *Academic Press, New York and London*, 1973.
30. Brezis, H. Functional Analysis, Sobolev Spaces and Partial Differential Equations. *Springer-Verlag New York*, 2011.
31. Quarteroni, A. and Valli, A. Numerical Approximation of Partial Differential Equations, *Springer Series in Computational Mathematics 23*, 1994.
32. Gunzburger, M. D. Finite Element Methods for Viscous Incompressible Flows: A Guide to Theory, Practice, and Algorithms (Computer Science and Scientific Computing), *Computer Science and Scientific Computing, Academic Press*, 1989.